Embedded Optical Fiber Bragg Grating Sensor in a Nonuniform Strain Field: Measurements and Simulations

by K. Peters, M. Studer, J. Botsis, A. Iocco, H. Limberger and R. Salathé

ABSTRACT—This paper investigates the use of embedded optical fiber Bragg gratings to measure strain near a stress concentration within a solid structure. Due to the nature of a stress concentration (i.e., the strong nonuniformity of the strain field), the assumption that the grating spectrum in reflection remains a single peak with a constant bandwidth is not valid. Compact tension specimens including a controlled notch shape are fabricated, and optical fiber Bragg gratings with different gage lengths are embedded near the notch tip. The form of the spectra in transmission varies between gages that are at different distances from the notch tip under given loading conditions. This variation is shown to be due to the difference in the distribution of strain along the gage length. By using the strain field measured using electronic speckle pattern interferometry on the specimen surface and a discretized model of the grating, the spectra in transmission are then calculated analytically. For a known strain distribution, it is then shown that one can determine the magnitude of the applied force on the specimen. Thus, by considering the nonuniformity of the strain field, the optical fiber Bragg gage functions well as an embedded strain gage near the stress concentration.

KEY WORDS—Optical fiber sensor, Bragg grating, embedded sensor, strain distribution, nondestructive evaluation

The use of optical fiber gages to measure temperature, strain, or even detect fracture in a material has great potential due to their relatively small size, sensitivity and immunity to electrical fields.[1] Surface-mounted optical fibers, for example, have been used in a variety of strain gage applications.[2] Furthermore, due to their dimensions, optical fiber gages can be embedded unobtrusively into materials, particularly composites already containing fiber reinforcements. However, once an optical fiber is embedded, the interpretation of the gage response becomes more complex due to the effects of interface between the fiber and the material, as well as the multiple components of strain applied to the fiber.[3–6] The problem is further complicated when the strain field surrounding the gage is not sufficiently uniform with respect to the scale of the gage length.

As an example, the optical fiber Bragg grating (OFBG) sensor permits the localized measurement of axial strain in an optical fiber. In comparison with a simple optical fiber displacement gage, the response of the OFBG sensor is only affected by the strain (or temperature) field at the location of the grating and not along other portions of the optical fiber. This property makes the OFBG sensor especially useful for measuring localized phenomena such as the strain conditions near a region of fracture.[7]

The conventional treatment of the OFBG as a strain gage assumes that the reflected spectrum is a single distinct peak whose shift is linearly proportional to the applied strain. Naturally, this assumption is only valid if the gage length is sufficiently small so that the strain can be considered to be constant along this length. For the measurement of strains in large structures far from bolts, joints, inclusions and so on, this does not present a problem. However, this scaling argument cannot be reduced to an arbitrarily small scale, since the minimum length of an OFBG sensor is limited due to the physical conditions of the fabrication process and the requirement of several grating periods to generate reflection.[8] In addition, the magnitude and dimensions of the strain gradient may not be known a priori, hence the need for an experimental measure. Once a strain distribution is applied to the grating, the peak broadens and, depending on the severity and form of the gradient, may even divide into multiple peaks. Rather than acting simply as signal noise, however, the shape changes of the response spectrum can serve as distributed sensor information.[7,9] In the ideal case, the resolution of this measurement is on the order of a few grating periods. The goal of this paper is to demonstrate such a measurement for an embedded sensor near a varying stress concentration.

We first review the analytical response of a uniform periodic OFBG to constant and nonconstant strain fields. Next, we detail the preparation and loading of compact tension specimens, chosen because the strain field is highly nonlinear and yet controllable near the stress concentration, with embedded Bragg gages of different gage lengths. The spectra in transmission differed between these specimens under identical loading conditions. This variation is shown to be due to the distribution of strain along the gage length. The spectrum in transmission is then calculated analytically for the applied

K. Peters is an Assistant Professor, Department of Mechanical and Aerospace Engineering, North Carolina State University, Raleigh, NC 27695. M. Studer is a Doctoral Student, and J. Botsis is a Professor, Department of Mechanical Engineering, Swiss Institute of Technology, CH-1015 Lausanne, Switzerland. A. Iocco is an Engineer, Network Planning Department, DiAx, CH-8304 Wallisellen, Switzerland. H. Limberger is a Group Leader, and R. Salathé is a Professor, Department of Microengineering, Swiss Institute of Technology, CH-1015 Lausanne, Switzerland.

Original manuscript submitted: May 20, 1999.
Final manuscript received: October 10, 2000.

nonuniform strain field measured using electronic speckle pattern interferometry on the surface of the specimen. The simulations correspond with the measured spectra, demonstrating that the spectra can be used to measure the local strain, even under highly nonuniform conditions.

OFBG

The OFBG is a permanent periodic modulation in the index of refraction along a given length of the optical fiber core, fabricated by ultraviolet irradiation of the fiber.[10] Due to the coupling between forward- and backward-propagating modes, some wavelengths of light are reflected rather than transmitted by the fiber at the location of the grating. The reflected, or similarly transmitted, spectrum is sensitive to physical changes in the grating due to applied strain or temperature. The following sections review the transmission and reflection properties of a grating subjected to an applied strain field, both uniform and nonuniform.

OFBG As Strain Gage

OFBGs have been used to measure the strain at a known location within a structure.[11,12] In general, a uniform periodic grating is used to determine the strain averaged over the gage length. Within limits, this gage length can be quite short, making the measurement practically at a point for large structures. An example of the change in index of refraction along the gage length and the reflected spectrum of such a uniform grating is shown in Figs. 1(a) and 1(b). The parameters of this spectrum can be adjusted by changing the parameters of the OFBG during the writing process. Two essential parameters in this case are the wavelength at maximum reflectivity, λ_B (often called the Bragg wavelength), and the bandwidth, $\bar{\lambda}$ (defined as the distance between the two first minima). These parameters are given by

$$\lambda_B = 2n_{eff}\Lambda \tag{1}$$

$$\frac{\bar{\lambda}}{\lambda_B} = \frac{1}{n_{eff}}\sqrt{\left(\zeta\overline{\delta n_{eff}}\right)^2 + (\lambda_B/L)^2}, \tag{2}$$

where Λ is the period of the grating, L is the gage length, n_{eff} is the effective mode index, $\overline{\delta n_{eff}}$ is the mean induced change in n_{eff} (averaged over a grating period) and $\zeta\overline{\delta n_{eff}}$ is the amplitude of the induced index change.[10] Thus, as a strain gage, λ_B is measured at the reference "zero strain" state and then measured once axial strain, e_{zz}, is applied to the gage. It is assumed that the temperature remains constant (or is otherwise compensated) and that the other components of strain are negligible. The shift in λ_B as a result of the change in grating period is then linearly proportional to the applied strain,[1]

$$\frac{\Delta\lambda_B}{\lambda_B} = \left[1 - \frac{1}{2}n_{eff}^2(p_{12} - \nu(p_{11} + p_{12}))\right]\varepsilon_{zz} = (1 - p_e)\varepsilon_{zz}, \tag{3}$$

where p_{11} and p_{12} are photoelastic constants and ν is the Poisson's ratio of the fiber. Included in this equation is the assumption that the applied strain, ε_{zz}, is constant along the gage length. For the case in which this assumption does not apply, the geometrical approach of measuring $\Delta\lambda_B$ is no longer applicable, since the form of the spectral response changes.

This assumption becomes critical if one wants to use the OFBG to measure strain near a stress concentration or any other significant strain gradient. One approach to avoiding this problem is to fabricate the grating with a gage length sufficiently small so that the strain does not change significantly along the length. However, this technique is limited by the physical conditions of the fabrication process. In practice, gages of length approximately 0.3 mm have been written.[8] In addition, the magnitude of the strain gradient may not be known a priori. Thus, the following section presents an approximating technique to treat the spectral response of the gage subjected to a strain gradient. This technique will be used later to analyze the experimental results.

Response to Nonuniform Strain Field

To determine the reflection and transmission spectra of a uniform grating subjected to a nonuniform strain field, we will treat the problem in reverse. Thus, we consider the grating as an initially nonuniform grating (i.e., the initial period is a nonconstant function along the fiber axis) subjected to a uniform strain field. This approach is chosen due to the formulation already developed for such "chirped" gratings.[13] Here, the piecewise continuous formulation of a chirped grating is reviewed while introducing the effects of applied strain.

Defining z as the variable along the fiber axis, the variation of the effective index of refraction of a chirped OFBG can be written as

$$\delta n_{eff}(z) = \overline{\delta n_{eff}}\left\{1 + \zeta\cos\left[\frac{2\pi}{\Lambda_o}z + \phi(z)\right]\right\}, \tag{4}$$

where Λ_o is the initial grating period at zero strain and $\phi(z)$ describes the change in grating period along the length.[13] As demonstrated in the previous section for a uniform grating, the applied strain induces a change in both the grating period and the mean index. Because the two effects can be linearly superimposed, at least for a piecewise continuous strain field because it is locally uniform, we can include the two effects by applying an effective strain, $(1 - p_e)\varepsilon_{zz}(z)$, to the grating period. Thus, we can write the grating period as

$$\Lambda(z) = \Lambda_o\left[1 + (1 - p_e)\varepsilon_{zz}(z)\right]. \tag{5}$$

The effective mode index is

$$\delta n_{eff}(z) = \overline{\delta n_{eff}}\left\{1 + \zeta\cos\left[\frac{2\pi}{\Lambda_o[1 + (1 - p_e)\varepsilon_{zz}(z)]}z\right]\right\}. \tag{6}$$

Combining eqs (6) and (4) and solving for $\phi(z)$ results in

$$\phi(z) = -\frac{2\pi}{\Lambda_o}\frac{(1 - p_e)\varepsilon_{zz}(z)}{[1 + (1 - p_e)\varepsilon_{zz}(z)]}z. \tag{7}$$

Figures 1(c) and 1(d) show $\delta n_{eff}(z)$ and the associated reflected spectrum for such a chirped grating. In general, $\varepsilon_{zz}(z)$ can be an arbitrary function of z; thus, we need to be able to determine the reflected spectrum for any function $\varepsilon_{zz}(z)$. Unfortunately, such a detailed approach is often not efficient, as the numerical integration is time consuming, which precludes the use of the OFBG as a gage in real time. Thus,

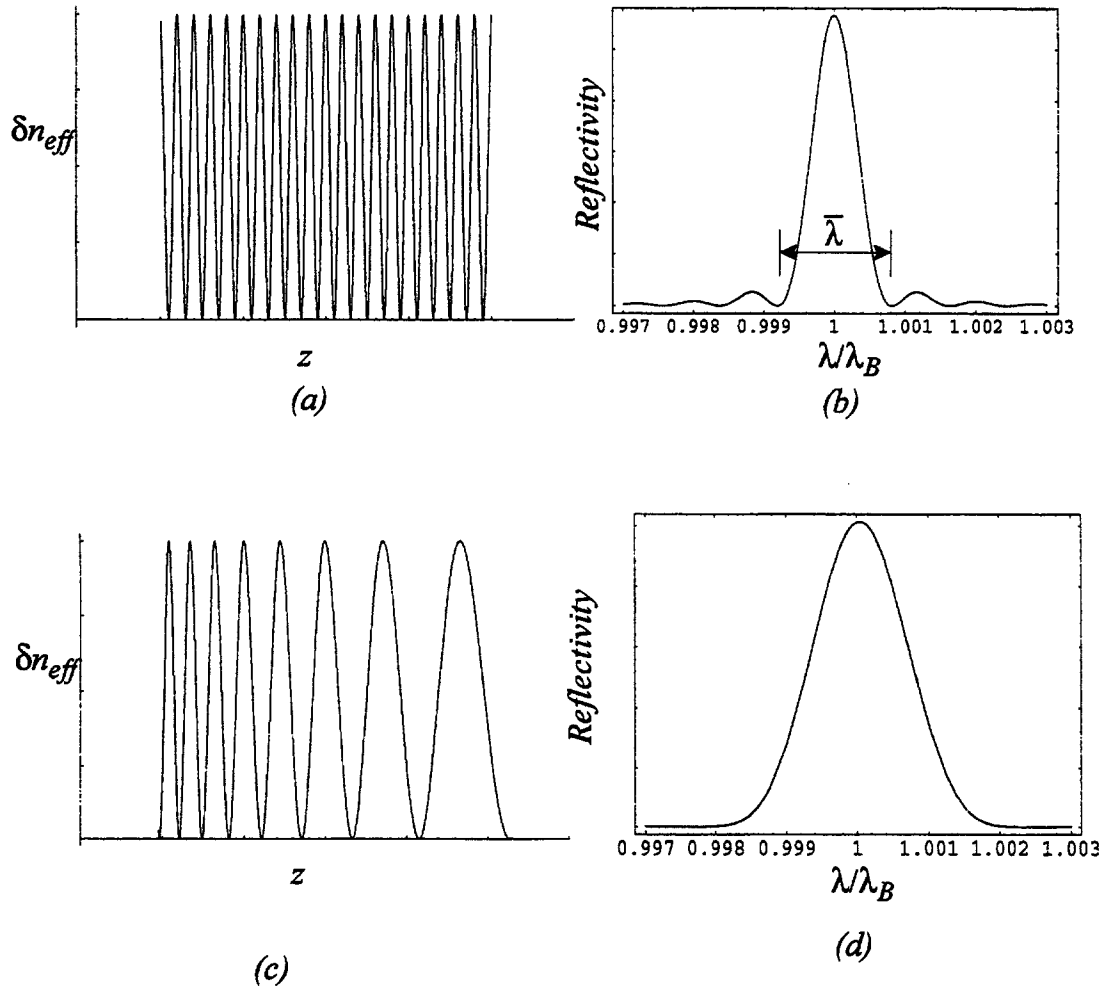

Fig. 1—(a) Variation of the index of refraction of a uniform optical fiber Bragg grating (size of grating period with respect to length of grating is exaggerated to show features), (b) reflected spectrum of uniform grating, (c) variation of index of refraction of "chirped" grating, (d) reflected spectrum of chirped grating

we approximate $\varepsilon_{zz}(z)$ as a piecewise continuous function to facilitate the calculation.[14]

Using coupled mode theory, one can write the optical response matrix of a uniform grating, F, as the transformation between the input and output spectra,

$$\begin{bmatrix} P_o \\ N_o \end{bmatrix} = F \begin{bmatrix} P_I \\ N_I \end{bmatrix}, \tag{8}$$

where P_I is the input wave traveling in the positive direction, N_I is the input wave traveling in the negative direction and P_o and N_o are the output waves in the positive and negative directions, respectively. For an OFBG, this matrix is given by

$$F(\lambda) = \begin{bmatrix} \cosh[\gamma_B(\lambda)\Delta z] - i\frac{\hat{\sigma}(\lambda)}{\gamma_B(\lambda)}\sinh[\gamma_B(\lambda)\Delta z] & -i\frac{\pi\nu\overline{\delta n_{eff}}}{\gamma_B(\lambda)\lambda}\sinh[\gamma_B(\lambda)\Delta z] \\ i\frac{\pi\nu\overline{\delta n_{eff}}}{\gamma_B(\lambda)\lambda}\sinh[\gamma_B(\lambda)\Delta z] & \cosh[\gamma_B(\lambda)\Delta z] + i\frac{\hat{\sigma}(\lambda)}{\gamma_B(\lambda)}\sinh[\gamma_B(\lambda)\Delta z] \end{bmatrix} \tag{9}$$

$$\hat{\sigma}(\lambda) = \frac{2\pi n_{eff}}{\lambda} - \frac{\pi}{\Lambda} + \frac{2\pi}{\lambda}\overline{\delta n_{eff}}$$

$$\gamma_B(\lambda) = \sqrt{\left(\frac{\pi}{\lambda}\nu\overline{\delta n_{eff}}\right)^2 - \hat{\sigma}^2(\lambda)},$$

where Δz is the length of the grating segment considered.[13] The OFBG is then divided into a series of M smaller gratings each subjected to a uniform strain field, as shown in Fig. 2. The optical response matrix is known for each section and termed F_i. One can write the total response matrix of the grating as the multiplication of each individual matrix,

$$F = F_M \cdot F_{M-1} \cdot \ldots \cdot F_1. \tag{10}$$

The applicability of the piecewise continuous strain field assumption is limited by the gradient of the actual strain field. To apply the coupled mode equation approximation to an OFBG segment, the length of the segment must be greater than a few periods long.[13] Thus, the minimum length of a division of the piecewise continuous distribution, $l_{\min}$, is given by

$$l_{\min} \gg \Lambda. \tag{11}$$

This does not pose a problem for the measurements presented

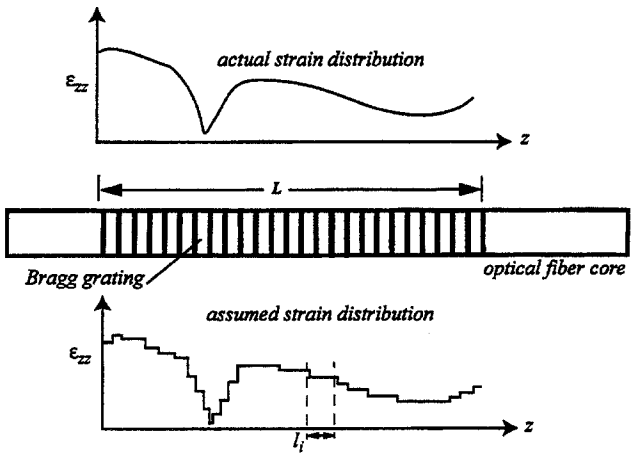

Fig. 2—Piecewise continuous assumed strain distribution along length of optical fiber Bragg grating. l_i is the length of the ith portion, $\sum_{i=1}^{M} l_i = L$, note that $l_i \neq l_j (i \neq j)$

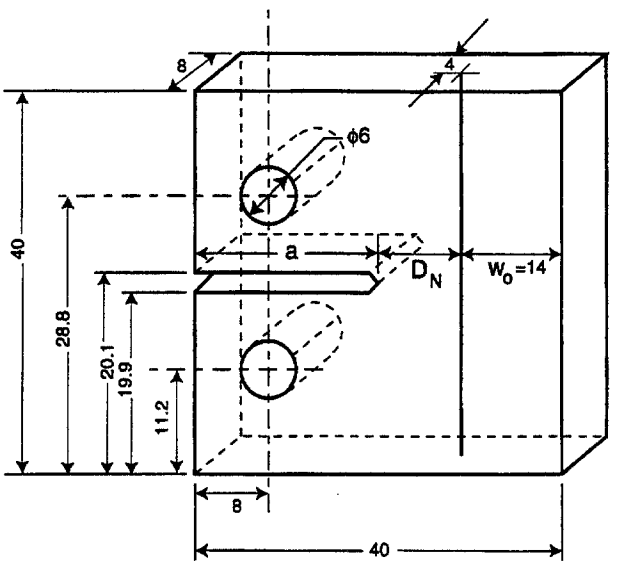

Fig. 3—Compact tension specimen with embedded fiber (all dimensions in mm). The variables a, notch length, and D_N, distance between fiber and notch tip, vary between individual specimens

in this paper, as reasonable results were obtained for $l_{min} = 0.1$ mm using gratings with initial periods of 538 nm.

The question of the uniqueness of the F matrix with respect to a given strain distribution, and hence the uniqueness of the sensor response, is not treated here. Although the response varies with both strain magnitude and distribution, different combinations of the two could potentially lead to identical spectra. We consider that some information about the stain field is known a priori, although this issue needs to be addressed in future work. In addition, we do not consider the problem of automating the treatment of the spectral response, since for now we only use the gages in a laboratory environment.

Experimental Procedure and Results

To test the response of an OFBG near a stress concentration, a series of compact tension specimens of epoxy were fabricated including embedded OFBG sensors. The stress concentration was introduced through a machined notch, for which the shape of the tip was repeatable. The response of the sensor was then measured for two gage lengths and various strain distributions (controlled by varying the distance between the optical fiber and the notch tip).

Gage Calibration

The OFBGs were first calibrated by applying displacements to the free fiber. This calibration was performed for several identical gratings to verify the repeatability of the grating fabrication and gage properties. For these gratings, the sensitivity is $p_e = 0.264 \pm 0.024$. Afterwards, uniaxial traction specimens were prepared (following the procedure described below for compact tension specimens). Three specimens were fabricated, the first with a gage length of 10 mm, the second also with a gage length of 10 mm and the third with a gage length of 2.5 mm. The last two gages were treated with silane along the stripped length to create a strong bond between the glass fibers and the epoxy.[15] The thickness and width of the uniaxial tension specimens were chosen to be the same as those of the compact tension specimens so that the residual stresses, dependent on the form of the mold, would be the same. The specimens were loaded until the fiber fractured within the specimen, at approximately 0.8 percent strain. Within this strain range, the gage response remained linear and did not significantly vary between specimens, indicating that the silane treatment does not significantly affect the response of the grating (i.e., there is no slipping between the fiber and matrix without the treatment).

Specimen Preparation and Loading

The OFBGs were then embedded in epoxy compact tension (CT) specimens. A Dow Chemical three-part epoxy was used composed of DER 330, DER 732P and DEH 24 mixed in a 35:15:10 weight ratio. The epoxy was cured for 24 h at room temperature. The dimensions of the CT specimen are shown in Fig. 3. The optical fibers used are 125 μm diameter standard monomode optical fibers provided by Alcotel, Switzerland, into which OFBGs were written at the Institute of Applied Optics at the Ecole Polytechnique Fédérale de Lausanne. The OFBGs were generated by exposing the fiber, after H_2 loading to increase its photosensitivity, to a 248 nm pulsed Excimer laser through a phase mask with a period of about 1.076 μm. The fluence per pulse was 250 mJ/cm^2, and the total irradiation dose was 4.7 kJ/cm^2. All fibers were stripped of the acrylate coating along the embedded length, whereas some were also treated with silane. For this treatment, the fibers were dipped in an ethanol-based silane solution, rinsed with ethanol and then allowed to dry 24 h in a dry container before embedding. The specimens were fabricated in molds under vacuum to remove any air bubbles from the liquid epoxy before hardening. The modulus of the epoxy was measured independently to be 2.6 GPa. The modulus of the optical fibers is considered to be 72 GPa, the accepted value in the literature.[15] To prevent breaking of the fiber at the exit points of the specimen, a plastic tube was added that entered into the specimen approximately 3 mm at each end of the fiber, sufficiently far from the grating.

After removing the specimen from the mold, the notch was machined. The distance between the notch tip and the fiber was measured to ± 0.05 mm using a microscope. As

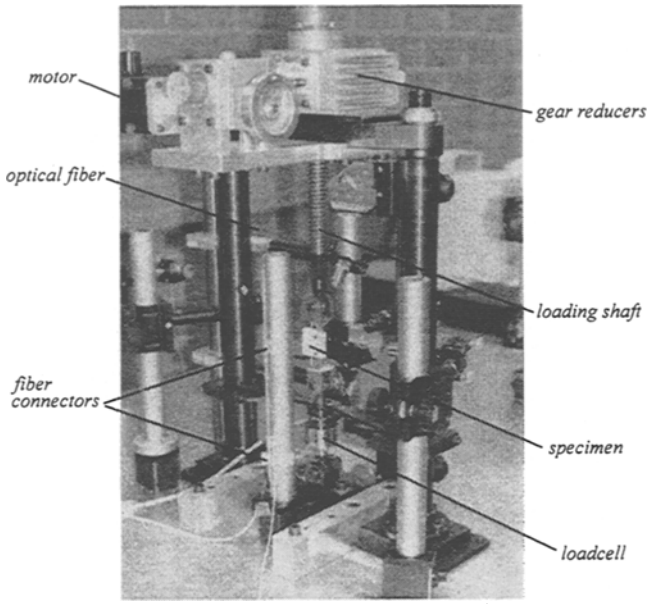

Fig. 4—Tensile loading frame for compact tension specimens. Also visible are CCD camera and optical components for the electronic speckle pattern interferometry measurements

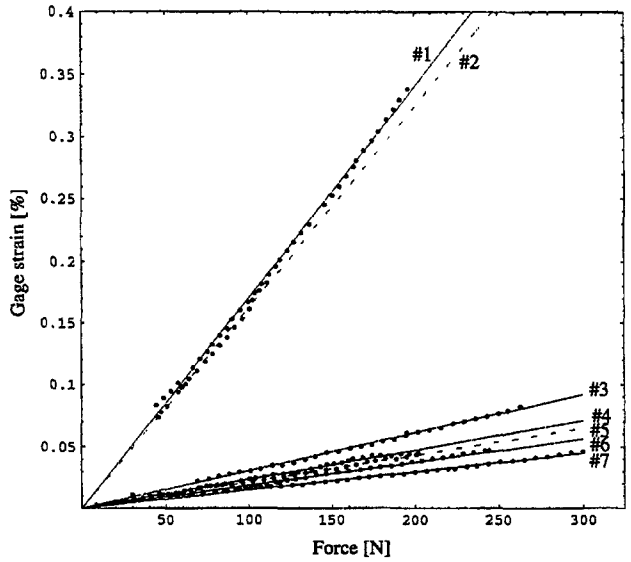

Fig. 5—Plot of gage strain (percentage) versus applied force for initial seven specimens. For specimens 1 and 2, D_N = 2 mm, whereas for specimens 3-7, D_N = 6 mm. Dashed lines represent specimens for which the gage was not treated with silane before fiber was embedded

the distance D_N was varied by extending the notch, the notch length, a, was not a constant for these experiments. Instead, the distance w_o, shown in Fig. 3, remained constant.

The specimens were loaded in traction in a loading frame constructed to rest on a vibration-isolated optical table so that the in-plane surface displacements could be measured simultaneously using electronic speckle pattern interferometry. This measurement provides an independent verification of the strain distribution in a later section. This loading frame, with a mounted specimen, is shown in Fig. 4. The load is displacement controlled and provided by a continuous-current motor. The force is measured using a standard load cell. The displacement of the loading pins was measured independently using dial gages, whereas the signal of the OFBG was monitored using a tunable laser light source with a step of 10 pm and a photodetector to measure the output intensity. Finally, the effect of change in room temperature between various tests was eliminated by connecting an optical fiber containing a reference OFBG in series with the measurement fiber. The reference grating signal was measured at the start of each test to determine the wavelength shift of the spectra due to the temperature.

Preliminary Experiments

The first series of experiments were performed after embedding optical fibers containing OFBGs of length 10 mm into epoxy CT specimens. A series of seven specimens were fabricated. The gage strain versus applied force for each specimen is shown in Fig. 5. For specimens 1 and 2, $D_N = 2$ mm, whereas for the other specimens, $D_N = 6$ mm. Although the response was linear for each gage, the variation in slope was as much as 50 percent for the specimens with $D_N = 6$ mm. This is believed to be due to several manufacturing errors in the specimens. For instance, the epoxy modulus was measured between specimens prepared at different times and found to vary as much as 7 percent. However, the largest error is that in D_N due to the machining of the notch. For the tests 3-7, D_N varied between 6.0 mm and 6.3 mm. Thus, it was determined that D_N could not be accurately controlled; however, it could be accurately measured to $\pm$ 0.05 mm. The center of the 10 mm gage was measured to be 0.2 mm from the axis of the notch.

In addition, some gages were treated with silane before embedding to create a bond between the glass fiber and the epoxy.[15] The response of the treated gages is shown as dotted lines in Fig. 5, whereas the untreated gages are represented by dashed lines. The difference in gage strain versus force slope was not significant between the treated and untreated gages. Thus, because the strain applied to the fibers was relatively low as compared to the maximum strain applied during the calibration tests, the epoxy residual stress was sufficient to prevent slipping of the gage. During the later tests, the effect of this residual stress was eliminated by adjusting the zero of the calibration curves for the embedded gages. As the response of the embedded gages was always linear, this approach is reasonable.

Measurement of Strain Field near the Notch Tip

From these initial experiments, it was evident that the results of different specimens could not be compared without an uncertainty due to manufacturing errors. Thus, for the following tests, a single specimen was fabricated for each gage length, and the distance D_N was varied by elongating the notch. Two different gage lengths were used. The first length of 10 mm was embedded in a specimen, labeled A, whereas the second length of 1.5 mm was embedded in a specimen, labeled B. Both fibers were treated with silane before embedding.

As demonstrated later, the response of the 1.5 mm gage remained a single peak with a constant bandwidth throughout the range of applied loading. Thus, the gage length of 1.5 mm was sufficiently small for the strain fields measured during

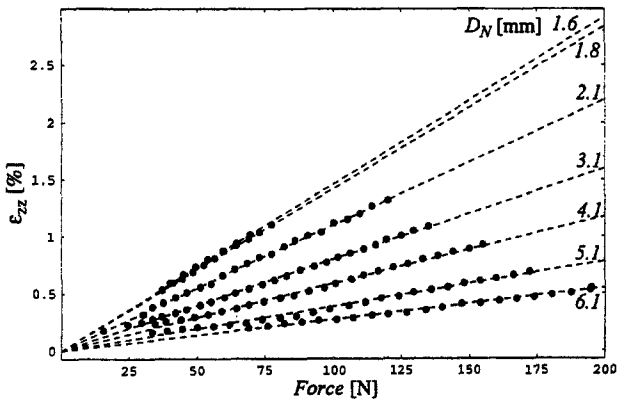

(a)

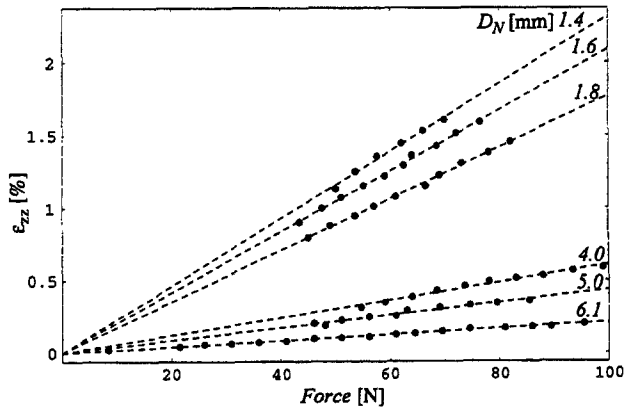

(b)

Fig. 6—Plots of sensor strain versus applied force for various distances between fiber and notch tip, D_N: (a) specimen A, gage length 10 mm; (b) specimen B, gage length 1.5 mm

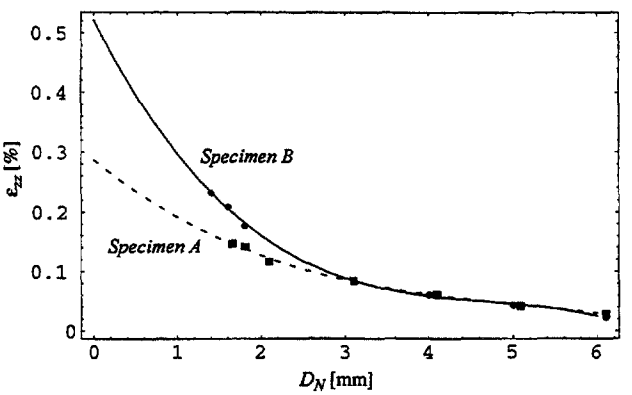

Fig. 7—Strain per unit force as a function of D_N plotted for the two specimens. Gage length of 10 mm is represented by a dashed line, gage length of 1.5 mm is represented by a solid line and curve is polynomial fit to data

the following experiments and can be used as a reference to compare with the 10 mm gage length.

Figures 6(a) and 6(b) show the sensor strain, calculated from the wavelength shift of the principle peak using eq (3), versus applied force for specimens A and B, respectively. Each response was measured for several values of D_N. As shown, the response was linear for each test. The slopes of these curves are then plotted in Fig. 7 as a function of D_N. A curve is also drawn for each specimen to show the trend of the data. Because the average theoretical axial strain along the embedded gage length of 10 mm, $\overline{\varepsilon_A}$, is different than that for 1.5 mm, $\overline{\varepsilon_B}$, the data for specimen B are multiplied by the ratio $\overline{\varepsilon_A}/\overline{\varepsilon_B}$ so that the two curves can be compared. Although the geometry is identical for each specimen, the sensor response diverges significantly for $D_N < 3$ mm. When the gage is far from the stress concentration, i.e., $D_N > 3$ mm, the measured strain is the same for the two gages. Thus, the divergence is due to the difference in gage length and not the specimen fabrication.

The effect of gage length is immediately visible when one regards the spectra in transmission for the two gages as a function of D_N. Figure 8 shows several examples of such spectra. Figures 8(a), 8(b) and 8(c) are taken from the output of specimen A, with a gage length of 10 mm. In Fig. 8(a), for which $D_N = 5.1$ mm, the fiber is relatively far from the notch tip. Initially, the spectrum is a principal peak with a small secondary one, due to the residual stresses created during the setting of the epoxy and the machining of the notch. As the load is increased, the spectrum divides into two distinct peaks of approximately the same order. The same behavior is demonstrated in Fig. 8(b), where $D_N = 2.1$ mm, although the spectrum divides into as many as four individual peaks. A more extreme case develops in Fig. 8(c), where the initial spectrum at $P = 0$ is already extremely nonuniform. In contrast, Fig. 8(d) shows the output response of specimen B, with a gage length of 1.5 mm. In this plot, $D_N = 1.8$ mm, the same distance as Fig. 8(c). However, for the short gage length, the response remains a single peak. Note that the maximum applied force for Figs. 8(c) and 8(d) is the same.

Analytical Calculation of Gage Response

Motivated by the difference in gage responses, as described above, the spectral response of the grating was calculated taking into consideration the actual strain field applied to the grating. For this purpose, the ε_{zz} strain field (where z is the longitudinal axis of the optical fiber) at the surface of the specimen was calculated from vertical displacement measurements using electronic speckle pattern interferometry on the surface of the specimen.[16] These calculations were performed simultaneously with the OFBG measurements. It is assumed that the strain field in the interior of the specimen, specifically at the plane of the optical fiber, is proportional to that on the surface. In addition, the axial strain component transferred from the matrix to the optical fiber, ε_{zz}, is considered to be significantly greater than the other strain components transferred; thus, the gage response is calculated based on a uniaxial applied strain field as provided earlier. This assumption was later justified by the lack of visible birefringence effects in the grating signals (i.e., the appearance of two distinct peaks not derivable from the applied axial strain field). These assumptions are shown to lead to excellent simulations of the grating spectra in transmission due to a nonuniform applied strain field. The measured surface distribution of ε_{zz} is plotted in Fig. 9 for several values of D_N. In this plot, $z = 0$ corresponds to the center of the grating. Using the matrix approach of eqs (8)-(11), the distributions at $D_N = 2.1$ mm were then used to calculate the grating response for a series of applied loads, P.

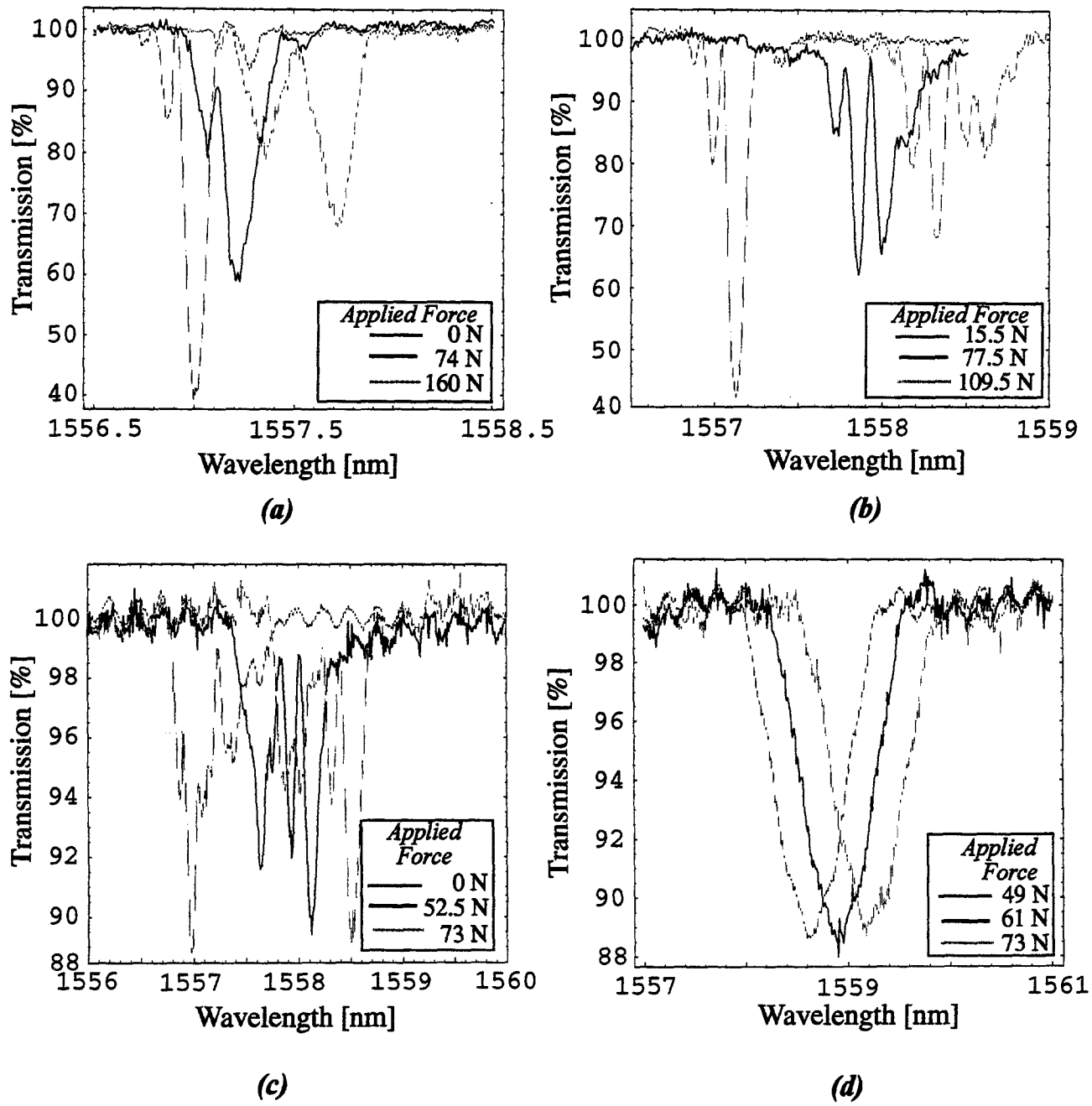

Fig. 8—Examples of spectra in transmission measured during experiments. Specimen A (gage length 10 mm): (a) D_N = 5.1 mm, (b) D_N = 2.1 mm, (c) D_N = 1.8 mm; specimen B (gage length 1.5 mm): (d) D_N = 1.8 mm. Undulations in examples (c) and (d) are due to data acquisition card signal

Defining the function taken from the plot in Fig. 9, at a given distance D_N, as $\varepsilon^*_{zz}(z)$, the strain applied to the grating is then given by

$$\varepsilon_{zz}(z) = \alpha\varepsilon^*_{zz}(z) + \gamma, \tag{12}$$

where α and γ are constants. Assuming that the system remains linear elastic, α and γ are proportional to the force, P. The grating period can then be calculated from eq (5) as

$$\Lambda(z) = \Lambda_o(1 + \alpha\varepsilon^*_{zz}(z) + \gamma). \tag{13}$$

This simulation was performed for each of the measured spectra at D_N = 2.1 mm. For each case, the coefficients α and γ were chosen to best fit the appropriate measured spectra. The effects of these two coefficients are independent: α changes the form of the spectrum whereas γ induces a global shift of the spectrum. Figure 10 shows several examples of the calculated spectra (dashed) plotted with the measured spectra (solid) for comparison. As observed, the evolution of the transmission spectra with increasing load was well modeled by the analytical calculations. The simulated spectra

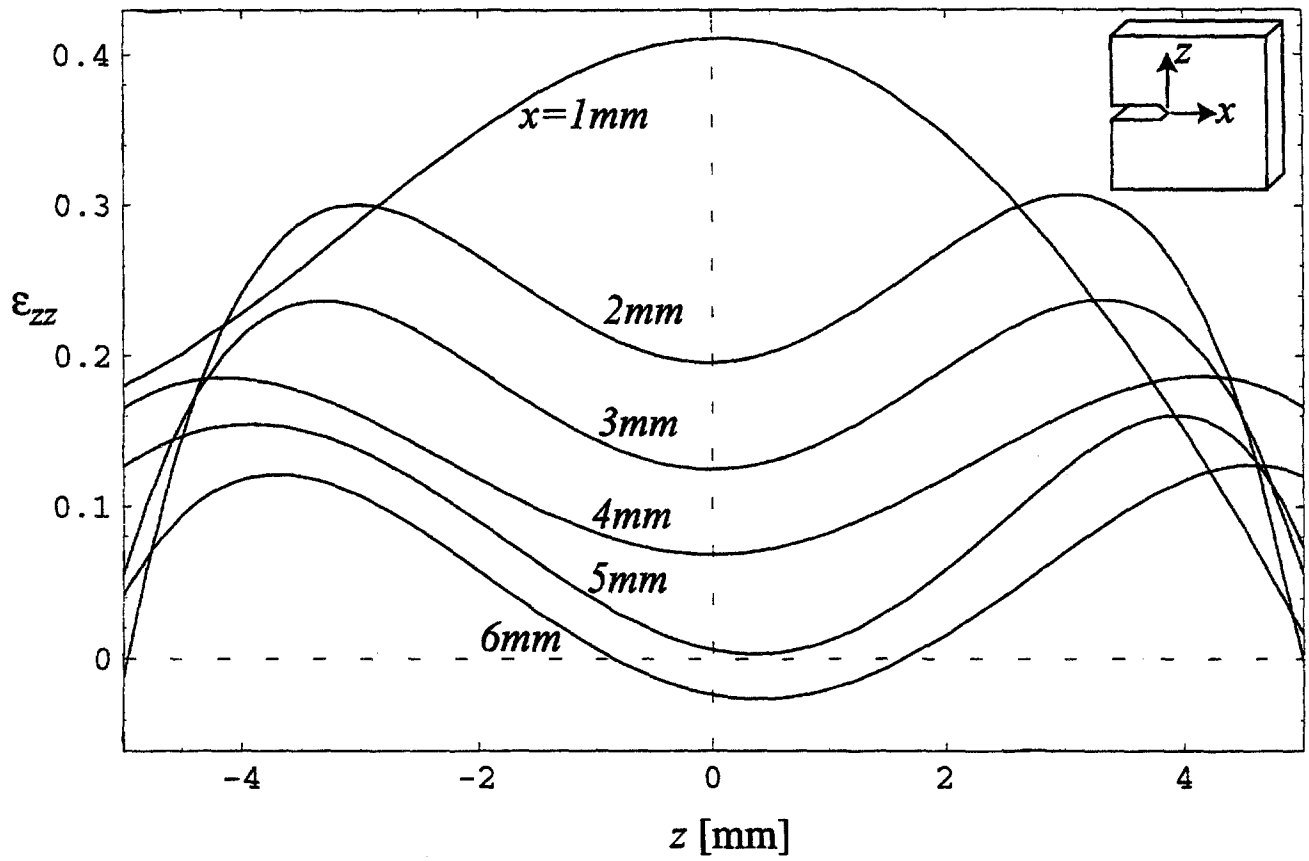

Fig. 9—Plot of measured strain distribution along gage length on surface of specimen from electronic speckle pattern interferometry. Distribution is plotted for several fiber locations

show the same development of multiple peaks of different amplitudes. After $P = 46$ N, the furthermost peak to the right shows a loss of percentage transmission near the peaks as compared to the simulations. This is most probably due to a local gradient that is too severe, since the loss follows the same region. Because this reduction does not appear in later tests with the same specimen, i.e., at $D_N = 1.8$ mm, it is not due to a local permanent damage in the grating. This same loss appears in the principal peak once $P = 90$ N.

After performing the simulations, the final step is to verify that the coefficients α and γ chosen to best fit the measured spectra are truly proportional to P. Figure 11 shows the values of α and γ plotted with respect to the applied force, demonstrating that α and γ vary linearly with P. The linear fit, plotted for each graph, does not pass completely within the error bars of each measurement. This is probably due to the fact that the best fit for each spectrum was chosen visually and could be improved through a strict mathematical definition. Thus, in summary, if the form of the strain distribution along the gage length is known, one can use the spectra of Fig. 10 to determine the applied load at each spectrum.

Conclusions

In this article, it was demonstrated that the OFBG functions well as an embedded strain sensor, even when the strain distribution along the gage length is not constant. For a uniform strain distribution, one can measure the shift in the wavelength of maximum reflectivity (the Bragg wavelength), which is linearly related to the strain. However, when the applied strain field is not constant with respect to the gage length, the grating output spectrum no longer undergoes a simple global wavelength shift but changes form as well, as demonstrated experimentally. Using a piecewise continuous model of the strain distribution along the grating length, the measured output spectrum of an OFBG was then verified analytically for several nonuniform strain distributions.

While the simulations demonstrate that the response can be calculated analytically if the strain distribution is known, the inverse problem has not yet been solved for a highly nonuniform yet arbitrary stress distribution. This inverse problem presents several difficulties including the question of the uniqueness of a given solution and its error sensitivity to noise in the spectrum. The inverse problem is the subject of future work.

As demonstrated, the OFBG permits a distributed measurement along a known segment of the optical fiber whose length and location can be controlled during the grating fabrication. Due to this feature, the gage has the potential to measure the local effects due to debonding in composite materials, particularly those containing glass fibers. As a specific example, work is currently in progress to directly measure the forces applied by reinforcing fibers bridging a matrix crack in a composite material.

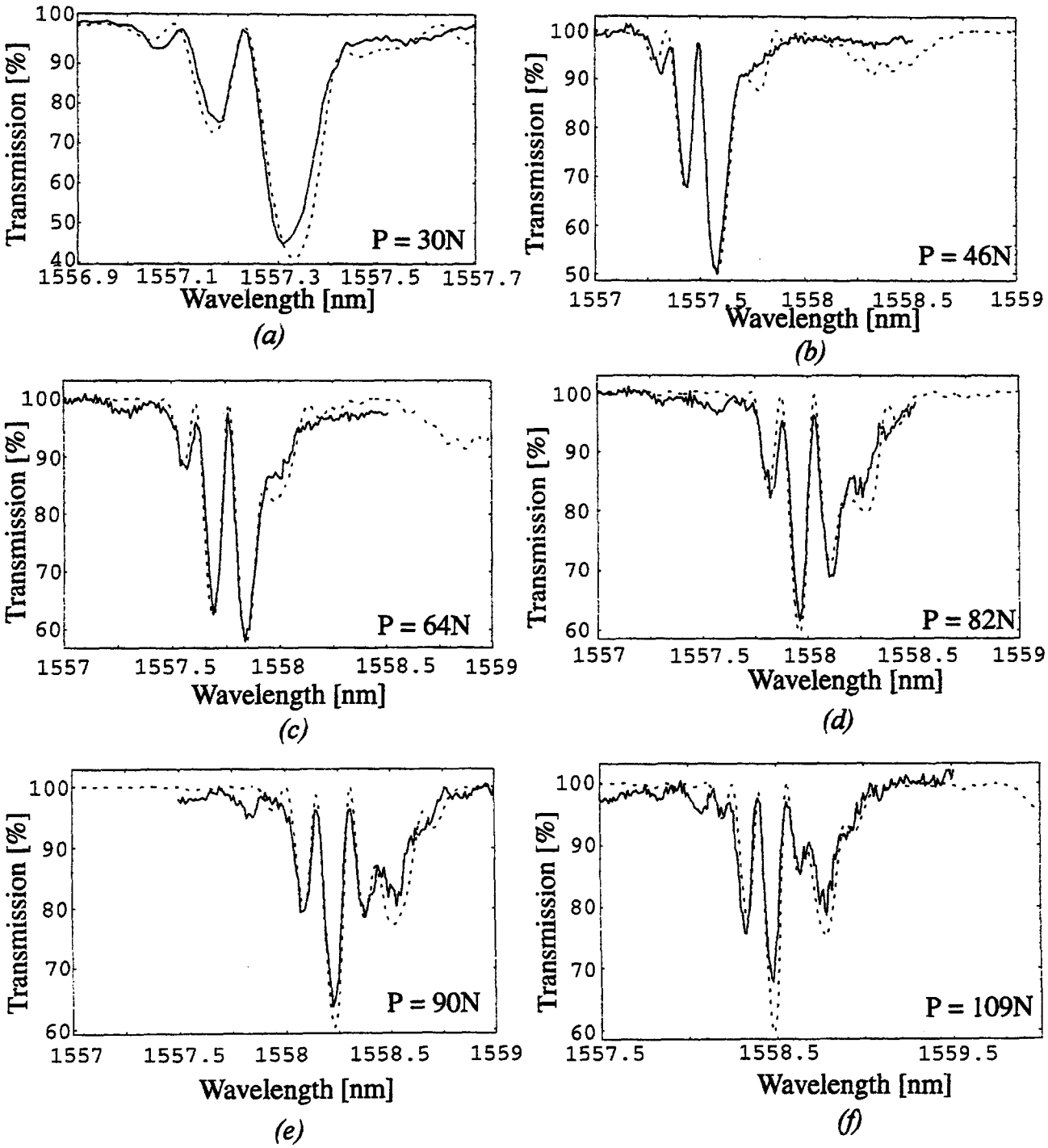

Fig. 10—Examples of numerical simulations of optical fiber Bragg grating spectra in transmission accounting for nonuniform distribution. Solid lines represent experimental data for a gage length of 10 mm for $D_N = 2.1$ mm at an applied force of (a) 30 N, (b) 46 N, (c) 64 N, (d) 82 N, (e) 90 N, (f) 109 N. Dashed lines represent the calculated gage response using measured strain distribution at the surface of the specimen

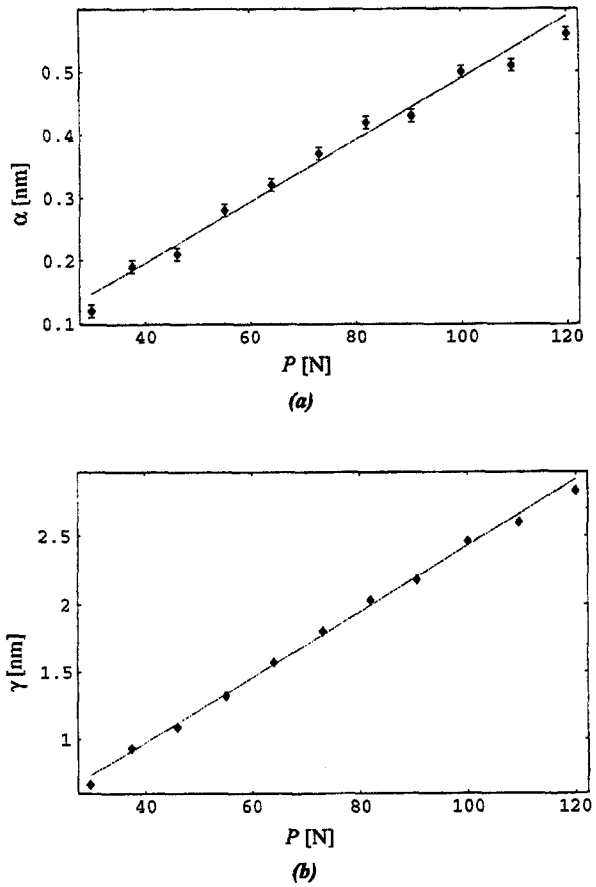

Fig. 11—Plots of fitting coefficients for simulation of grating spectra: (a) α, (b) γ. Linear fit to data is also shown. Error bars for γ are too small to be visible

Acknowledgments

The authors wish to acknowledge the financial support of the Swiss National Science Foundation.

References

1. Measures, R., "Smart Composite Structures with Embedded Sensors," Composites Eng., **2**, *597–618 (1992).*

2. Butter, C.D. and Hocker, G.B., "Fiber Optic Strain Gauge," Appl. Opt., **17**, *2867–2869 (1978).*

3. Miller, M., Case, S., Carmen, G., Schmid, C.A., May, R.G., and Claus, R.D., "Validation of Axial Strain Transfer from a Composite Laminate to Embedded Optical Fiber Sensors," Proc. SPIE, **1798**, *19–29 (1992).*

4. Pak, Y., "Longitudinal Shear Transfer in Fiber Optic Sensors," Smart Mat. Struct., **1**, *57–62 (1992).*

5. Piggott, M.R., "Interface Properties of Fiber-reinforced Polymers," Composite Applications: The Role of Matrix, Fiber, and Interface, T. Vigo and B. Kinzig, eds., VCH, New York, 230–251 (1992).

6. Sirkis, J. and Lu, I., "On Interphase Modeling for Optical Fiber Sensors Embedded in Unidirectional Composite Systems," Adapt. Struct. Mat. Sys., **35**, *419–426 (1993).*

7. Huang, S., Ohn, M., LeBlanc, M., and Measures, R., "Continuous Arbitrary Strain Profile Measurements with Fiber Bragg Gratings," Smart Mat. Struct., **7**, *248–256 (1998).*

8. Limberger, H.G., Fonjallaz, P.Y., and Salathé, R.P., "Spectral Characterization of Photoinduced High Efficient Bragg Gratings in Standard Telecommunication Fibers," Electr. Lett., **29**, *47–48 (1993).*

9. Volanthen, M., Geiger, H., Cole, M.J., and Dakin, J.P., "Measurement of Arbitrary Strain Profiles within Fibre Gratings," Electr. Lett., **32**, *1028–1029 (1996).*

10. Bennion, I., Williams, J.A.R., Zhang, L., Sugden, K., and Doran, N.J., "UV-written In-fibre Bragg Gratings," Opt. Quant. Electr., **28**, *93–135 (1996).*

11. Davis, M., Bellemore, D., Putnam, M., and Kersey, A., "High Strain Monitoring in Composite-wrapped Concrete Cylinders Using Embedded Fiber Bragg Grating Arrays," Proc. SPIE, **2721**, *114–123 (1996).*

12. Simonsen, H., Paetsch, R., and Dunphy, J., "Fiber Bragg Grating Sensor Demonstration in Glass-fiber Reinforced Polyester Composite," Proceedings of the First European Conference on Smart Structures And Materials, 73–76 (1992).

13. Erdogan, T., "Fiber Grating Spectra," J. Lightwave Tech., **15**, *1277–1294 (1997).*

14. Yamada, M. and Sakuda, K., "Analysis of Almost-periodic Distributed Feedback Slab Waveguides via a Fundamental Matrix Approach," Appl. Opt., **26**, *3474–3478 (1987).*

15. Carmen, G. and Sendeckyj, G., "Review of the Mechanics of Embedded Optical Sensors," J. Composites Tech. Res., **17**, *183–193 (1995).*

16. Jones, R. and Wykes, C., Holographic and Speckle Interferometry, Cambridge University Press, New York (1989).